Kinetic effects on particle morphology and size distribution during batch precipitation

T. A. Ring

Powder Technology Laboratory, Ecole Polytechnique Fédérale de Lausanne, CH-1015 Lausanne, Switzerland

Abstract

This paper reviews the effect of growth and aggregation kinetics on particle shape and size distribution of batch precipitations. Crystal growth kinetics at each crystal surface determine the final crystal shape. These processes are affected drastically by impurities. Impurities typically used to alter crystal shape fall into the following categories: anions, cations, ionic surfactants, non-ionic surfactants and chemisorbed species. These impurities absorb in different ways on specific crystal faces, changing their growth kinetics and thus altering the crystal shape. Non-ionic polymer surfactants are effective in preventing aggregation by steric stabilization. When aggregation occurs, aggregate shapes are fractal. The mean size of precipitated particles and their size distribution are also discussed in view of various kinetic growth mechanisms.

Introduction

The morphology of a precipitated powder is important when its application is considered. For example, the specific surface area of powdered drugs affects absorption rate; the particle shape (and size) of a pigment influences its color, and the length to diameter ratio of a powdered reinforcement influences the strength and toughness of composite materials. These are only a few of the many examples where the precipitated particle morphology plays an important role in determining the properties of products. In addition, powder purity is to some degree influenced by particle morphology, since more irregular particle shapes trap solvent and other impurities more effectively.

Crystal shape

The shape of a crystal (*i.e.*, its crystal habit) can be either thermodynamically or kinetically controlled. However, thermodynamic control of crystal habit is only important for crystals grown at very low supersaturation ratios (*i.e.*, $S < 1.000\,1$). These crystals tend to be of a mineralogical origin. In most other cases, the rate of the slowest growing crystal faces gives rise to the crystals' shape.

Equilibrium shape

Gibbs [1] was the first to offer a thermodynamic description of the equilibrium shape of a crystal, where the total free energy of a crystal is the sum of the free energies associated with its volume, surfaces, edges and corners. Gibbs showed that the edges and corners had an effect only when the crystal was small and the surface free energy decreased in proportion to the crystal size. For crystals of the same volume, the equilibrium shape will occur at the minimum value of the total surface energy (*i.e.*, $E_T = \Sigma\gamma_i A_i$); where γ_i is the specific surface energy of the ith face with a surface area A_i. Wulff [2] established that for a crystal of a fixed weight, only one shape can correspond to the lowest free energy.

When a crystal has assumed its equilibrium shape, there exists within the crystal a point, shown in Fig. 1, to which the perpendicular distances from all faces, h_i, are proportional to their specific surface energy γ_i. Any other possible non-equilibrium face has a surface energy such that a plane drawn with the corresponding orientation and distance from this point of intersection would be entirely outside the crystal. This theorem corresponds to the following formula:

$$\frac{h_1}{\gamma_1} = \frac{h_2}{\gamma_2} = \frac{h_i}{\gamma_i} \tag{1}$$

When an equilibrium-shaped crystal forms, the

0032-5910/91/$3.50

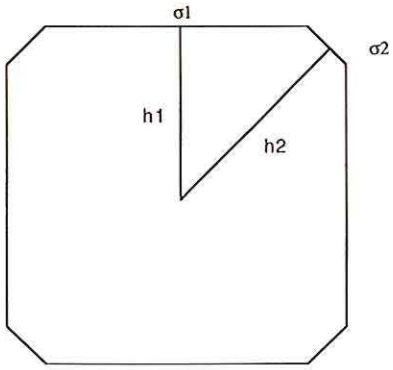

Fig. 1. Equilibrium crystal shape [4].

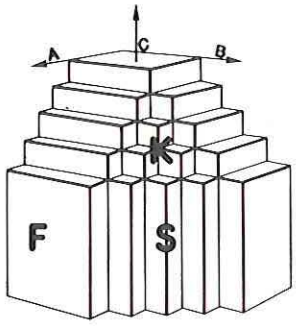

Fig. 2. Flat (F), stepped (S) and kinked (K) faces corresponding to the directions parallel to A, B and C crystallographic directions [7].

growth rate of each ith face is proportional to its surface energy. Because of their high growth rate, the high surface energy surfaces with their high growth rate will have the smallest surface area. They are also rougher, which supplements the higher growth rates. Wulff's theorem has been confirmed by careful experiments by Valetan [3] with small crystals ($\approx 10\ \mu$m).

Figure 2 shows an idealized cubic crystal with flat F faces, stepped S faces and kinked K faces. The rougher S and K faces grow very quickly compared with the F faces, because the distance that the growth unit must diffuse along the surface to be incorporated into the crystal structure is shorter on the S and K faces than on the F face. For this reason, these S and K faces are rarely, if ever, observed. The crystal habit is dominated by the slow growing F faces. From a fundamental knowledge of the crystal structure, it is possible to predict the slow growing F faces and thus the equilibrium crystal structure.

The value of this theory of crystal-habit equilibrium is limited due to the fact that normal crystal growth takes place at non-equilibrium conditions. However, Gibbs notes that for macroscopic crystals, the free energy associated with the driving force for precipitation will be larger than changes in free energy due to departures from the crystals's equilibrium shape. The shape of these crystals will depend on kinetic factors, which are affected by crystal defects, surface roughing, solvent type, impurities in the solvent and the actual precipitation conditions. Therefore, when a crystal retains its equilibrium shape, it simply means that either the 'kinetically controlled crystal habit' is the same shape as the equilibrium shape or that the crystal is grown at near-equilibrium conditions.

Kinetic shape

The rate determining step for the growth of the F faces of a crystal determines its kinetic shape. The S and K faces will almost grow faster than the F faces. The only exception to this rule is when an impurity is absorbed onto a S or K face; this will drastically reduce the growth rate of a S or K face to a level below that of an F face. These impurity effects are discussed later. Growth rates of different F faces often exhibit different dependences on the supersaturation ratios, and the crystal size R, as shown in Table 1.

A power law approximation for the growth rate $\mathrm{d}R/\mathrm{d}t|_i$ of each ith face as a function of the saturation ratio S has been suggested by many authors [4, 17]. This means

$$\left.\frac{\mathrm{d}R}{\mathrm{d}t}\right|_i = k_i S^{mi} \tag{2}$$

which is written in terms of a rate constant k_i and the exponent m_i which depends on the growth mechanism and the actual growth conditions. Therefore, the relative growth rates for two faces, denoted 1 and 2, would be

$$\frac{\left.\frac{\mathrm{d}R}{\mathrm{d}t}\right|_1}{\left.\frac{\mathrm{d}R}{\mathrm{d}t}\right|_2} = \frac{k_1 S^{m_1}}{k_2 S^{m_2}} \tag{3}$$

If the individual growth rates have the form suggested in Fig. 3, then face 2 will be the slowest growing face and control the crystal habit at low supersaturation, while face 1 will control the crystal habit for the higher levels of supersaturation. This type of behaviour has been verified for many real systems. One example is the precipitation of potassium iodide from aqueous solutions, where Kern [8] showed that two different crystal morphologies result from precipitating above and below a supersaturation of 1.14. Other aqueous precipitations also exhibit this behavior [5].

To complicate matters, during a batch precipitation, the supersaturation ratio decreases as the crystallisation proceeds. This can lead to a change in crystal habit and growth mechanism with time.

TABLE 1. Summary of bulk growth kinetics. Crystal growth rate dR/dt as a function of the saturation ratio S and the particle radius R. $dR/dt = C^* f(S)g(R)$

Growth mechanism	C	$f(S)$	$g(R)$	Ref.
Diffusion, bulk	$\frac{vD}{C_{eq}}$	$S-1$	1/R	[16]
Mono-surface nucleation	$\beta_A D\, d^{-1}$	$\exp\left(\frac{\Delta G_s^*}{3k_B T}\right)^a$	R^2	[4]
Poly-surface nucleation	$\frac{Dd}{(C_{eq})^{2/3}}$	$(S-1)^{2/3}\exp\left(\frac{\Delta G_s^*}{3k_B T}\right)^a$	1	[4]
Screw dislocation	$\frac{D_s n_{se}\beta}{(y_0^2 p)}$	$\frac{S^2}{S_1}\tanh\left(\frac{S_1}{S}\right)^b$	1	[15]
Heat conduction	$\frac{vk_H k_B T^2}{\Delta H_f}$	$\ln S^c$	1/R	[4]

[a] $\Delta G_s^* = \frac{\beta_L{}^2 \gamma_e{}^2 d^2}{(2\beta_A k_B T \ln S}$

[b] $S_1 = \frac{Sy_0}{2y_s}$

[c] $\ln S = \int_{T_b}^{T} \frac{\Delta H_f}{RT^2}\, dT$

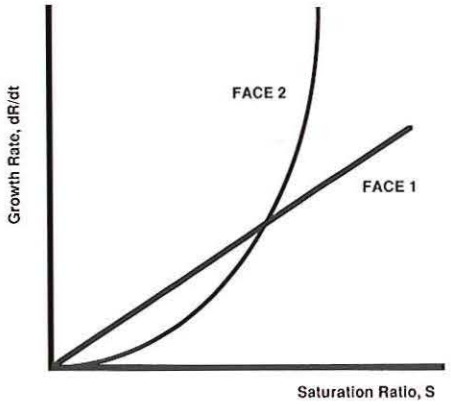

Fig. 3. Variation of growth rate, dR/dt, with supersaturation S for two F faces 1 and 2.

Since the rate constant k_i depends on temperature, the crystal habit can also be altered by drastic changes in temperature. The flow of solution around a crystal also influences its shape [7]. Crystal defects (*i.e.*, dislocations, twinning and inclusions) are also responsible for morphological changes. But the most important factor used in influencing crystal habit is impurity doping (intentionally or nonintentionally), which is discussed later.

Diffusion-controlled shape

A two-dimensional 'square crystal' is shown in Fig. 4. On the left are drawn curves with the same concentration in solution surrounding the crystal. On the right is drawn the shape of the crystal after different times. The growth rate is ≈60% higher at the corner than at the middle of the face [4], which leads to the conclusion that the corner of a crystal will tend to grow faster than the center of the faces when diffusion-controlled growth is the rate-limiting step. In the extreme, this leads to dendrite formation. Since the fast-growing corners have a thinner mass transfer boundary layer [4], the resistance to diffusion at the corner is less than that at the face. Several dendritic particles are shown in Fig. 5. In Fig. 5(b) for example, 12 axisymmetric dendrites are emerging from the cylindrical core of these fussy boehmite spheres.

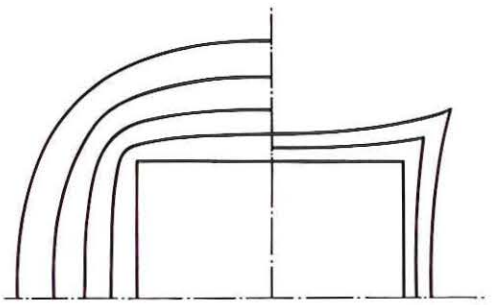

Fig. 4. Change in crystal shape by diffusional growth, On the left are given the concentration profiles around a 2-D crystal, while on the right is given the crystal shape at different times [4].

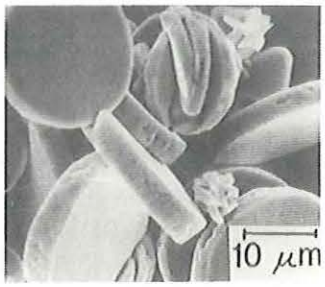

(a)

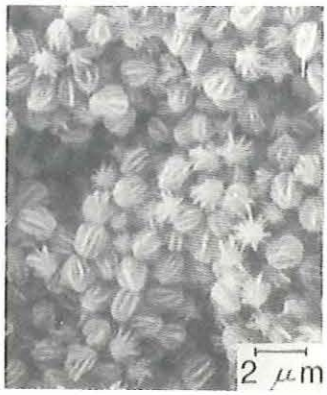

(b)

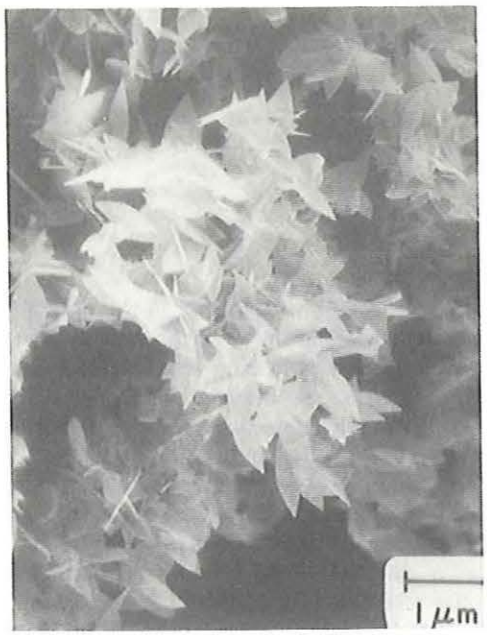

(c)

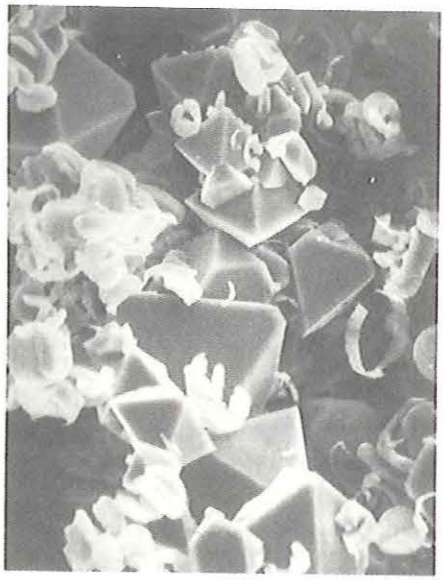

(d)

Fig. 5. Dendritic monosized particles precipitated by Matijevic: (a), hematite [48]; (b) boehmite; (c) vanadium oxide; (d) magnetite [49].

Surface nucleation-controlled shape

When surface nucleation is so slow that each layer on an F face originated from a single surface nucleus as shown in Fig. 6(a), the shape of the crystal will be controlled by the nucleation rate on the different F faces; that is, those with the lowest nucleation rate will have the largest surface areas. At higher levels of supersaturation, surface nuclei grow together as shown in Fig. 6(b), eventually flattening and completing the surface. Surface nucleation is highly dependent on the surface concentration of precipitating species [4], above a critical supersaturation ratio. Bulk diffusion to the surface will give a non-uniform surface concentration and the faces will no longer be planar and smooth, leading to spiral growth, as shown in Fig. 7(a), and step bunching, as shown in Fig. 8.

Growth spiral-controlled shape

Screw or spiral dislocations are commonly observed in many industrial precipitations from NaCl to sucrose. A screw dislocation will convert an F face to the shape of a pyramid or a cone. The angle θ of the cone for an Archimedian spiral can be calculated by [6]

$$\theta = \tan^{-1}\left(\frac{d}{y_0}\right) \tag{4}$$

Non-Archimedian growth spirals [7] occur due to: (i) a pair of dislocations of either like or opposite

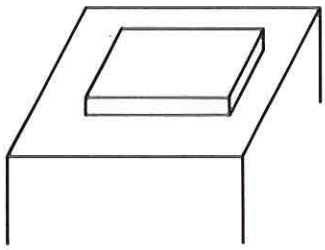

(a)

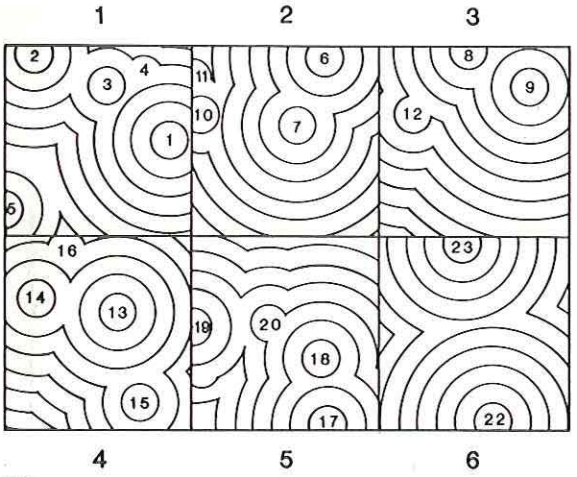

(b)

Fig. 6. Surface nucleation-controlled shape due to (a) 2-D nuclear growth, (b), Polynuclear growth [4].

sign as shown in Fig. 7(b), (ii) a group of dislocations lying along a line giving a hillock and 'wobbling' of the center of the spiral giving macroscopic spirals, as shown in Fig. 7(c). A single long hillock at the edges of Y Ba_2CuO_{7-x} superconducting crystals grown from flux as shown in Fig. 9 are responsible for their platelet shape [9]. At high levels of supersaturation, the above equation is not accurate, since several 'step bunching' spirals occur at once, giving larger values of θ.

Aggregate shape

Particles can aggregate by either Brownian-motion or shear-induced aggregation. With Brownian aggregation, diffusion of particles by Brownian motion causes particle collisions. With shear-induced aggregation, fluid movement—induced by an external source (e.g., a stirrer)—causes particle collisions. The change in the total number of particles per unit volume N_T, due to Brownian aggregation is given by

$$\frac{dN_T}{dt} = -4K N_T^2 \tag{5}$$

where K is the aggregation rate constant. This

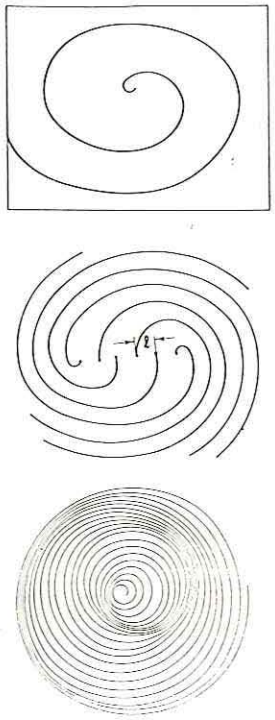

Fig. 7. Spiral shapes (a), simple spiral; (b) spiral due to a group of dislocations lying along a line; (c), macro spiral formation due to periodic motion of center [7].

expression has been shown to be in good agreement with experimental measurements [10].

To show how a population of particle sizes, $\eta(R, t) = N_k/R_k$, changes due to Brownian aggregation, a relationship can be derived [11] as follows:

$$\frac{d\eta(R,t)}{dt} = K \int_0^R \eta(x,t)\eta(R-x,t)\,dx - 2K\eta(R,t)N_T(t) \times \left[\frac{\overline{(x^2)}}{R^2} - \frac{2\bar{x}}{R} + 1\right] \tag{6}$$

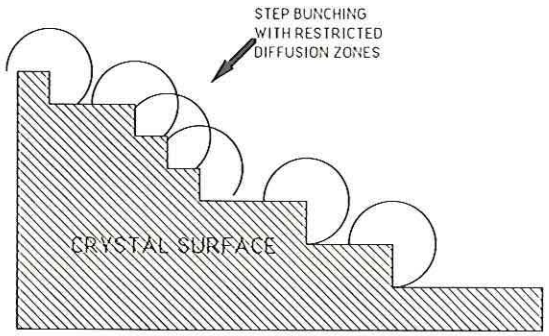

Fig. 8. Step bunching showing diffusion depletion zones (spherical) for each step.

where the aggregation rate constant is

$$K = \frac{k_B T}{3\mu W} \tag{7}$$

and W is the colloid stability factor. A value of $W = 1.0$ corresponds to the case where the rate of particle birth and death is equal to the particle collision rate (*i.e.*, a sticking probability of 1). The ith moment is described as follows:

$$\overline{(x^i)} = \frac{\int_0^\infty x^i \eta(x)\,dx}{\int_0^\infty \eta(x)\,dx} = \frac{\int_0^\infty x^i \eta(x)\,dx}{N_T} \tag{8}$$

For shear aggregation, the change in the total number of particles per unit volume N_T is given by:

$$\frac{dN_T}{dt} = -4\,K_s \sum_{k=1}^{p} k^* N_k^2 \tag{9}$$

where $K_s = 16\dot{\gamma}R_0^3/(3W)$ and R_0 is the initial particle radius, $\dot{\gamma}$ is the shear rate and p is the limit size which is a function of time t. A population of particle sizes, $\eta(R, t) = N_k/R_k$, changes due to shear aggregation [12] as follows:

$$\frac{d\eta(R,t)}{dt} = \frac{2}{3}R^2\dot{\gamma}\int_0^R x(R-x)\eta(x,t)\eta(R-x,t)\,dx - \frac{4}{3}\dot{\gamma}\frac{\eta(R,t)}{R}\int_0^\infty x(x+R)^3\eta(x,t)\,dx \tag{10}$$

An aggregate shape frequently observed in aggregative precipitation is seen in Fig. 10. This shape has evaded quantitative evaluation until the development of fractal mathematics [13]. The shape of the Brownian aggregates has been studied by computer modeling in two ways: (i) aggregation particle by particle [14, 15], as shown in Fig. 11(a) and (ii) aggregation cluster by cluster [16, 17], as shown in Fig. 11(b). These shapes turn out to be fractal [18], having the number of particles $N(R)$ inside a sphere of size R given by

$$N(R) \alpha R^{D_F} \tag{11}$$

where D_F is the fractal dimension. These computer models give a fractal dimension of 2.5 for particle/particle aggregation and 1.6 to 2.2, depending on the model used, for cluster/cluster

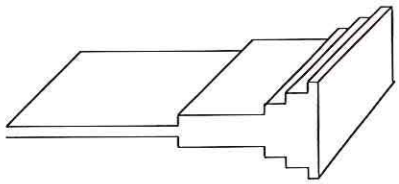

Fig. 9. Group of dislocations lying along a line giving an edge hillock.

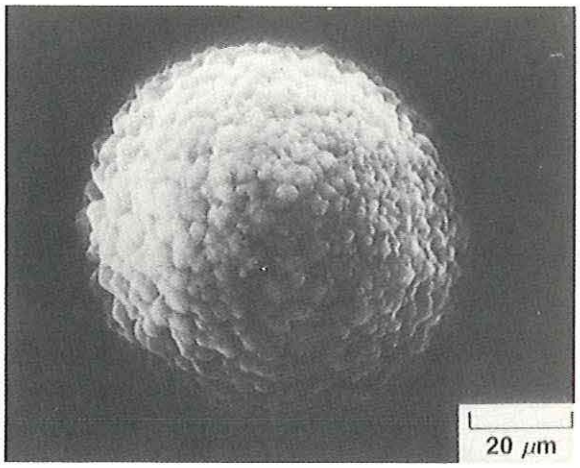

Fig. 10. Aggregate shape of particles grown in aqueous solution [51].

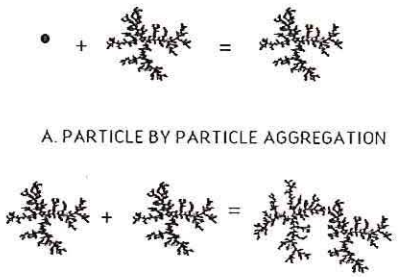

Fig. 11. Computer-generated fractal aggregate shape due to (a), particle–particle aggregation [50] ($D_F = 1.5$ in 2 D) and (b), cluster by cluster aggregation ($D_F = 1.2$ in 2 D).

aggregation. Figure 11 shows two-dimensional examples of a computer generated aggregates 'grown' under conditions of particle/particle aggregation (*i.e.*, $D_F = 1.5$ in 2D and 2.5 in 3D) and cluster–cluster aggregation (*i.e.*, $D_F = 1.2$ in 2D and 2.2 in 3D). Cluster/cluster aggregates are less dense (*i.e.*, greater porosity) on the average than particle/particle aggregates. If shear forces are used to mix the precipitating system, the shape of the aggregates may be much more compact like that shown in Fig. 10. This shape can also be

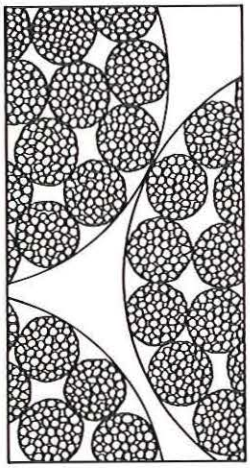

Fig. 12. Aggregate shape due to shear forces (schematic).

idealized as a fractal aggregate within and aggregate, as shown in Fig. 12, having a fractal dimension given by [19]

$$D_F = 4.0 + \frac{\ln P}{\ln S} \tag{12}$$

where S is the ratio between sizes and P is the packing fraction in each aggregate.

Crystal habit modification by impurities

All of the previously mentioned changes in crystal habit caused by kinetic factors can be drastically affected by the presence of impurities, which specifically absorb on a preferential face of a growing crystal. In the first example of crystal habit modification, which was described in 1783 by Romé de L'Isle [20], urine was added to a saturated solution of NaCl, changing the crystal habit from cubes to octahedra. A similar discovery was made by Leblanc [21] in 1788, when alum cubes were changed to octahedra by the addition of urine. Buckley [22] reviewed the effect of organic impurities on the growth of inorganic crystals from aqueous solution and Mullin [23] discussed the industrial importance of this practice.

Since crystal growth is a surface phenomenon, it is not surprising that impurities which concentrate at crystal faces will affect the growth rate of those faces and, hence, the crystal shape. With some surface active impurities, small traces (about 100 ppm) are all that is required to change crystal habit during crystallization. These impurities can (i) reduce the supply of material to crystal face, (ii) reduce the specific surface energy and (iii) block surface sites and pin the steps of the growing crystal.

The impurities which modify crystal habit fall into 4 categories:

(i) inorganic ions (either anions or cations),

(ii) ionic surfactants (either anionic or cationic),

(iii) non-ionic surfactants especially polymers and

(iv) chemisorbed species such as organic dyes.

Any of these surface active impurities has a propensity to adsorb on a specific crystal surface. The specific surface energy γ that results from the adsorption of Γ atoms (or ions) per unit area is given by Gibbs as

$$-\mathrm{d}\gamma = \Gamma k_B T(\mathrm{d} \ln a_2) \tag{13}$$

where a_2 is the solution activity of the impurity. This change in specific surface energy is also observed at the liquid–vapor interface which can be measured with a Langmuir trough as a change in the surface pressure. The adsorbed amount Γ is frequently related to the impurity activity by a Langmuir-type adsorption isotherm [23]

$$\Gamma = \Gamma_M \frac{ba_2}{1 + ba_2} \tag{14}$$

where $b(= K/a_1)$, which is related to the distribution coefficient K and the activity of the solvent a_1. The Langmuir adsorption isotherm is frequently used to describe the adsorption of ions and chemisorbing species but not polymers and ionic surfactants; however, a modified form of this equation can account for the adsorption of one polymer molecule in place of many solvent molecules [24] and micellization of ionic surfactants [25]. Each face of the crystal will be different with respect to adsorption. As a result, each crystal face will have its own adsorption isotherm Γ_i with its own values of Γ_{Mi} and b_i.

Experiments have been performed in which precipitations with surface active agents present were performed in a Langmuir trough to measure the surface pressure at the liquid–vapor interface of the surface active agent. These studies [26, 27] have shown that the crystal habit can be changed when there is sufficient surface coverage. These studies show the direct link between morphological changes during precipitation and the adsorption of surface active agents.

Habit modification by ionic and chemically binding impurities

As an example, Kern [28] discusses the adsorption of Cd ions in the habit modification of a NaCl and the adsorption of Pb in ppm levels on the habit modification of KCl. He postulates that the growth is suppressed on the {111} planes of NaCl due to a Cd layer that completely covers

that face of the crystal. This Cd adsorption preference is caused by the similarities between the {111} planes of NaCl and the {111} planes of $CdCl_2$. Matijevic has noted changes in crystal habit due to anions in several systems [29]. According to Burrill [30], the adsorption of impurities at a particular surface decreases the area of the crystal face available for adsorption of solute molecules and, therefore, the growth rate of this surface. Mullin [31] and Leci suggests that impurity ions in the vicinity of the surface will: (i) reduce the effective surface supersaturation, (ii) retard diffusion and (iii) hinder the aggregation of growth units.

Cabrera and Vermilyea [32] note that the growth rate will decrease if the mean distance between strongly adsorbed impurities is comparable with the size of the critical surface nuclei (r^*). Therefore, large impurities will retard the growth of the crystal faces on which they adsorb. This trapping the impurity in the nearest step site is commonly referred to as 'step pinning', as shown in Fig. 13. Overgrowth of these pinned impurities lead to crystal defects. Albon and Dunning [33] have observed step pinning on sucrose crystals in the presence of raffinose impurities.

Chernov [34] suggests that there are two effects of impurities: (i) if an impurity is relatively small and mobile, it may reduce the number of kink sites and (ii) if an impurity is large and immobile, it may act as an obstacle for step movement (*i.e.*, step pinning). Reducing the number of kink sites will also decrease crystal growth. Chernov estimates that an impurity concentration of 100 ppm will drastically reduce the crystal growth rate. Slavnova [35] qualitatively confirmed Chernov's hypothesis. The effects of poisons on surface nucleation kinetics and the spiral shape are discussed by Sears [36].

Buckley [37] has classified many different impurity effects on crystal habit modifications. In most cases, as previously discussed, the presence of impurities decreases the growth rate of specific crystal faces, which lead to a change in the crystal habit, since the slowest growing faces dictate the final crystal morphology. In some exceptional cases, impurities can increase the growth rate of a particular crystal face. Such an increase may be caused by a decrease in the surface energy, thus reducing the size of the critical nucleus. This reduction in surface energy leads to an increase in surface nucleation rate which more than compensates for a decrease in the step velocity [38].

Impurities, such as ppm levels of Pb^{2+} in the precipitation of NaCl, can improve the quality of the crystals [39] and not enter into the crystal lattice. One per cent of Fe added to the precipitation of ammonium dihydrogen phosphate gave high-quality, impurity-free crystals which grew at ten times the rate of the pure solutions [33]. Impurities can also cause the appearance of crystal faces not observed in pure solutions. Hartman [40] has proposed that some impurities will cause step or kink faces to become flat, due to the adsorption of impurities at the 'rough surface', as shown in Fig. 14. Lateral growth is only possible at a step, which growth on this type of surface is similar to growth on an F face [41].

Habit modification by ionic surfactants

Each different type of crystal face has a different surface chemistry. For example, kaolin platelets have an edge which is predominately Al_2O_3 and a face which is predominately SiO_2. In this case, each of these crystal faces adsorbs ions from solution differently. A surface charge results which is due to the adsorption of positive and negative ions. The adsorption of one type of ion usually predominates at a certain pH (and concentration of other ions). A measure of the equilibrium constant for this adsorption is the iso-electric point (*i.e.*, the pH at which the particles do not move in an electric field), which is different for different surface chemistries as shown in Table 2.

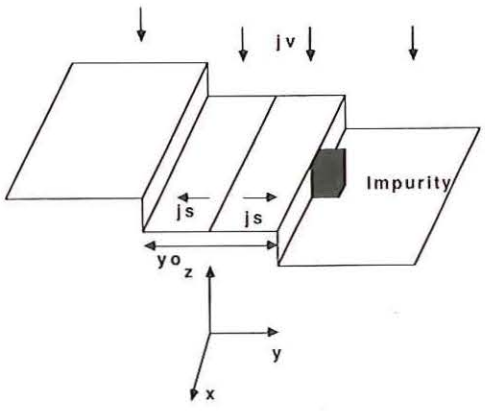

Fig. 13. Flux of a solute to a step with impurity pinning step movement.

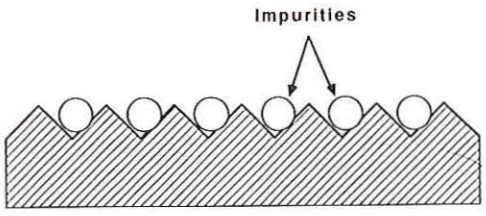

Fig. 14. Conversijon of S and K faces to F faces by adsorption of an impurity layer [7].

TABLE 2. Nominal isoelectric points of oxides

Material	Nominal Composition	IEP
Quartz	SiO_2	2
Soda lime silica glass	$1.00Na_2O0.58CaO.3.70SiO_2$	2–3
Potassium feldspar	$K_2O.Al_2O_3.6SiO_2$	3–5
Zirconia	ZrO_2	4–6
Apatite	$10CaO.6PO_2.2H_2O$	4–6
Tin oxide	SnO_2	4–5
Titania	TiO_2	4–6
Kaolin (edges)	$Al_2O_3.SiO_2.2H_2O$	5–7
Mullite	$3Al_2O_3.2SiO_2$	6–8
Chromium oxide	Cr_2O_3	6–7
Hematite	Fe_2O_3	8–9
Zinc oxide	ZnO	9
Alumina (Bayer process)	Al_2O_3	8–9
Calcium carbonate	$CaCO_3$	9–10
Magnesia	MgO	12

The growth rate for different crystal faces can be drastically changed by the specific adsorption [42] of ionic surfactant impurities at concentrations below their critical Micelle concentration. An example of this phenomenon is the use of anionic and cationic surfactants to change the habit of adipic acid crystals during precipitation [43]. As shown in Fig. 15, the addition of a cationic surfactant adsorbs on the negatively charged surfaces of adipic acid and limits their growth giving platelet-like crystals. Anionic surfactants will adsorb on the positively charged surfaces of the adipic acid crystals and limit their growth, giving needle-like crystals. This preferential and strong adsorption of ionic surfactant is frequently used industrially to control crystal morphology during precipitation.

Shape modification by non-ionic polymeric surfactants

If the crystals nucleated and grown in a supersaturated solution are colloidally unstable (*i.e.*, $W \approx 1.0$), they will aggregate when their number density is sufficiently high. Polymers that adsorb on the surface are used as precipitation additives to sterically stabilize the freshly precipitated particle against aggregation. Polymers typically exhibit a Langmuir-type adsorption isotherm [23]. At monolayer coverage (or some fraction thereof), aggregation is prevented [44]. In a batch reactor, the initial supersaturation is high, which leads to a high nucleation rate. These nuclei are small in diameter and have a huge surface area per unit volume. If the amount of polymer added is insufficient to stabilize this size of particle, aggregation will take place. With the same amount of polymer, the aggregation will stop when the particles have grown to a size (*i.e.*, a sufficiently low surface area per unit volume) where there is enough polymer to provide steric stabilization [38].

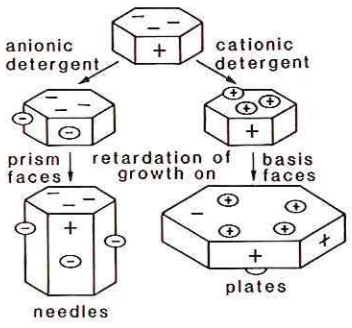

Fig. 15. Influence of ionic surfactants on the shape development of adipic acid crystals grown from aqueous solution [4].

In stirred-batch reactors, the shear forces will tend to compact the aggregates [45] as shown in Fig. 10. If cluster–cluster aggregation occurs, nuclei and first-generation aggregates will be incorporated into the final aggregate structure, as shown schematically in Fig. 12. This is the case [39] with TiO_2 particles precipitated from alcoholic solution of titanium ethoxide and water with polymer additions of hydroxylpropyl cellulose.

Crystal size distribution

In a batch precipitation, the growth rate affects the population size distribution $\eta(R, t)$ according to the population balance

$$\frac{\partial \eta(R, t)}{\partial t} + \frac{\partial\left[\frac{dR}{dt}\eta(R, t)\right]}{\partial R} = 0 \tag{15}$$

Using the growth rate functionality given from Table 1 of the form $g(R) = R^n$ in the population balance equation, with the initial condition

$$\eta(R, t = 0) = \eta^0(R) \tag{16}$$

the following solution [46] results

$$\eta(R, t) = \sum_{i=1}^{\infty} A_i g^{-1}(R) \exp[\lambda_i \int g^{-1}(R)\, dR] \times \exp[-c\lambda_i \int F(S)\, dt] \tag{17}$$

where A_i is a vector of coefficients corresponding to the eigenvalues λ_i. These coefficients are determined from the initial condition as follows:

$$A_i = \int_0^{\infty} \eta^0(R) g^{-1}(R) \exp[\lambda_i \int g^{-1}(R)\, dR] \tag{18}$$

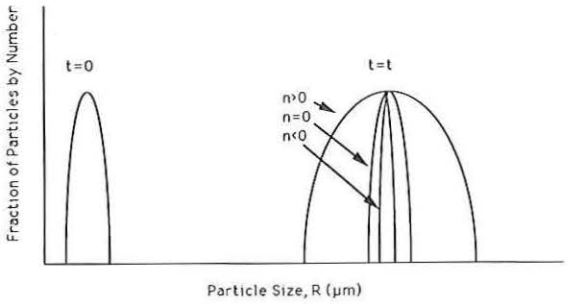

Fig. 16. Particle size distribution in a batch crystallizer with different size dependent growth rates (see Table 1 for values of n).

The second experimental term in eqn. (17) accounts for the decrease in the saturation ratio S as of function of time t. For $g(R) = R^n$, the size distribution of particles will (i) widen with time for $n > 0$, (ii) remain the same for $n = 0$ and (iii) get narrower for $n < 0$. The growth of size distributions with different values of n is shown in Fig. 16.

Aggregate size distribution

When the saturation ratio S is large, the nucleation is the most important process in the reduction of the concentration of precipitating species at the beginning of batch precipitation. At the high nucleation rate, aggregation plays an important role in the forming of the particles produced during precipitation when the colloid stability ratio W is small near 1.0. To account for aggregation in the population balance for batch precipitation, eqn. (15) must be combined with eqn. (6) as follows:

$$\frac{\partial \eta(R,t)}{\partial t} + \frac{\partial[\mathrm{d}R/\mathrm{d}t\ \eta(R,t)]}{\partial R} = K\int_0^R \eta(x,t)\eta(R-x,t)\,\mathrm{d}x - 2K_\eta(R,t)N_T\left[\frac{\overline{(x^2)}}{R^2} + \frac{2\bar{x}}{R} + 1\right] \quad (19)$$

This equation has no analytical solution. The following approximate solution [47] for the mean aggregate size λ as a function of time assumes that the most frequent collision is between nuclei and large aggregates and that the entire precipitating mass is precipitated as nuclei at time $t = 0$.

$$\lambda - \lambda_0 = R_0 \ln\left[1 + \frac{t}{t_{1/2}}\right] \quad (20)$$

where λ_0 is the initial aggregate size, often equal to R_0 [47], the nuclei size, and $t_{1/2}$ is the half-life for aggregation defined by

$$t_{1/2} = \frac{1}{\sqrt{K\eta^0(R)R_0}} \quad (21)$$

This equation has been shown to agree with experimental data by several authors when aggregation is the most important growth mechanism [40] (*i.e.*, $\beta = KN_T R_0/(\mathrm{d}R/\mathrm{d}t) > 1$). In this distribution, the nuclei and the aggregates coexist, giving a bimodal size distribution. Since particle aggregation is a diffusion-controlled process, it will have a size-dependent growth rate function $g(R) = 1/R$ and the width of the aggregate size distribution will decrease as the aggregates become larger, as shown in Fig. 16.

Conclusion

This article reviews the state of our knowledge concerning the shape and size distribution of precipitated particles. Crystal shape is discussed from the point of view of equilibrium and kinetic effects, the latter being most sensitive to impurities. The effects of the various types of impurities including anions, cations, anionic and cationic surfactants, chemically binding impurities and non-ionic polymeric surfactants are discussed separately. Each has an effect on growth and aggregation kinetics, giving rise to different crystal shapes. The kinetic effects on particle size distribution are discussed from the point of view of a population balance. The solution to the population balance gives the size distribution at various times after nucleation. Under some conditions, the size distribution widens as growth proceeds, while in other conditions, the size distribution narrows.

List of symbols

a	activity ($_1$solvent, $_2$solute)
A_i	area of ith crystal face, [L^2]
b	coefficient in Langmuir equation
C	concentration ($_{eq}$equilibrium), [M/L^3]
d	height of step, [L]
D	diffusivity of precipitating species, ($_s$surface), [L^2/θ]
E_T	total surface energy, [ML^2/θ^2]
$f(S)$	saturation ratio dependence on growth rate
$g(R)$	radius dependence on growth rate, [L^n]
G	Gibbs free energy, (*critical, $_s$surface), [ML^2/θ^2]
h_i	distance from point to crystal surface, [L]
ΔH	enthalpy, ($_f$fusion), [ML^2/θ^2]
k_H	heat transfer coefficient, [$ML/(\theta^3 \cdot K)$]
k_B	Boltzmann constant, 1.38×10^{-23}, [$ML^2/(\theta^2 \cdot K)$]
K	distribution coefficient for Langmuir equation

K aggregation rate constant, ($_s$shear) $[L^3/(\theta \cdot N_0)]$
R spherical particle size (radius), [L]
R_0 nuclei particle size, [L]
n_{sc} surface equilibrium concentration, $[M/L^3]$
N_i total number of particles of type i per unit volume, $[No./L^3]$
N_T total number of particles present per unit volume, $[No./L^3]$
p limit number for shear aggregation, $-$.
R_i particle size (radius) of ith particle, [L]
S saturation ratio, C/C_{eq}, $-$
t time $[\theta]$
$t_{1/2}$ $1/(KN_0)$, half-life for aggregation, $[\theta]$
T absolute temperature, [T]
x an integration variable for the range of particle sizes, [L]
$\bar{x}$ number, length mean diameter, [L]
(x^2) number, surface mean diameter, $[L^2]$
y_0 distance between steps, [L]
y_s mean distance travelled by solute molecules on face, [L]
W colloid stability factor, $-$

Greek symbols

β shape factor ($_A$area), ($_L$length,)
β ratio, aggregation rate to growth rate, $-$
γ specific surface energy of ith crystal face
γ shear rate, $[\theta^{-1}]$
Γ adsorbed density, ($_M$monolayer), $[M/L^2]$
η^0 constant nuclei population at time zero and size R_0, $[No./(L^3 \cdot L)]$
$\eta(R, t)$ number population density, $[No./(L^3 \cdot L)]$
λ_a size of aggregate growth unit (radius), [L]
λ_i. eigenvalues
θ angle of spiral cone
ν reciprocal of molar volume, $[L^{-3}]$
μ viscosity, $[M/(L \cdot \theta)]$

Note: Fundamental dimensions are defined as follows:
No. = number of particles
M = mass
L = length
θ = time
T = temperature

References

1 J. W. Gibbs, *Trans. Connecticut Acad. 3* 1875, 1878. See also J. W. Gibbs, *Collected Works*, Longmans, Green, New York, 1928.
2 G. Wulff, *Z. Krist., 34* (1901) 449.
3 J. J. P. Valeton, *Ber. d. Math.-Phys. Klasse d. Kgl. Sachs. Ges. d. Wiss. (Leipzig) 67* (1915) 1.
4 A. E. Nielsen, *Kinetics of Precipitation*, Pergamon Press, Oxford, 1964.
5 A. V. Belyutsin and V. F. Dvorikin, *Growth of crystals, 1* (1957) 139.
6 W. K. Burton, N. Cabrera and F. C. Frank, *Phil. Trans., A243* (1951) 299.
7 D. Erwell and H. J. Scheel, *Crystal Growth From High-Temperature Solutions*, Academic Press, New York, 1975.
8 R. Kern, *Growth of Crystals, 8* (1969) 3.
9 H. J. Scheel and Ph. Niedermann, *J. Crystal Growth, 94* (1989) 281.
10 K. J. Ives, in K. J. Ives (ed.), *The Scientific Basis of Flocculation*, Sijthoff and Noordhoff, The Netherlands, 1979, p. 37.
11 J. A. Dirksen and T. A. Ring, in G. Kotorz (ed.), *High-Tech Ceramics, Views and Perspectives*, Academic Press, London, 1989.
12 J. A. Dirksen, Private communication.
13 B. B. Mandlebrot, *The Fractal Geometry of Nature*, Freeman Press, San Francisco, 1982.
14 M. J. Vold, *J. Colloid Sci., 18* (1963) 684 and *J. Phys. Chem., 63* (1959) 1608.
15 D. N. Sutherland, *J. Colloid Sci., 25* (1967) 373.
16 R. Jullien, *J. Phys. Rev. A, 29* (1984) 997.
17 R. C. Ball and R. Jullien, *J. Phys (Paris) Lett. 45* (1984) L103.
18 J. Meakin, in H. E. Stanley and N. Ostronsky (eds.), *Random Fluctuations and Pattern Growth*, Academic Press, London, 1989.
19 G. Onoda and J. Tover, *J. Am. Ceramic Soc., 69* (1986) C-248-C250.
20 Romé de L'Isle, Cristallographie, Paris, 2nd edn., 1783, p. 379.
21 N. Leblanc, *Journ. de Phys., 33* 1788. *Ann. de Phys., 23* (1788) 375.
22 H. E. Buckley, *Crystal Growth*, Wiley, New York, 1951.
23 J. W. Mullin. *Crystallisation*, Butterworths, London, 2nd edn., 1972.
24 A. W. Adamson, *Physical Chemistry of Surfaces*, Wiley–Interscience, New York, 4th edn., 1982.
25 B-Y. Zhu, and T. Gu, 4th edn., *J. Chem. Soc. Faraday Trans, I., 85* (1989) 3813.
26 S. Mann, *Nature 332* (1988) 10.
27 S. Mann, B. R. Heywood, S. Rajam and J. D. Birchal, *Nature, 334* (1988) 25.
28 R. Kern, *Growth of Crystals, 8* (1969) 3.
29 E. Matijevic, *Langmuir, 2* (1986) 12.
30 K. A. Burril, *J. Crystal Growth, 12* (1972) 239.
31 J. W. Mullin and C. L. Leci, *Desupersaturation of Seeded Citric Acid Solution in a Stirred Vessel*, Proc. Joint meeting AIChE and 3rd IMIQ, Denver, Colorado, August 1970, Paper 39a; Chem. Eng. Progr. Symp. Nucleation Phenomena,
32 N. Carbrera and D. A. Vermilyea, in R. H. Doremus, B. W. Roberts, D. Turnbull (eds.), *Growth and Perfection of Crystals*. Wiley, New York and Chapman and Hall, London, 1958, p. 393.
33 N. Albon and W. A. Dunning, *Acta Cryst., 15* (1962) 115.
34 A. A. Chernov, *Sov. Phys. Usp., 4* (1961) 129.
35 E. N. Slavnovna, *Growth of Crystals, 1* (1958) 117; *2* (1958) 166.
36 G. W. Sears, *J. Chem. Phys., 29* (1958) 104.
37 H. E. Buckley, *Crystal Growth*, Wiley, New York, 1951.
38 G. W. Sears, *J. Chem. Phys., 29* (1958) 104.
39 P. H. Egli and S. Zerfoss, Disc. Faraday Soc., 5 (1949) 61.
40 P. Hartmann, *Growth of Crystals, 7* (1969) 3.
41 M. Ledérset and J. C. Monier, In *Adsorbtion et croissance cristalline*, Intern. Colloq. CNRS No. 152, Paris, 1965, p. 537.
42 B. E. Novich and T. A. Ring, *Langmuir, 1* (1985) 701.

43 A. S. Michaels and F. W. Taasch, Jr. *J. Phys. Chem*, *65* (1961) 1730.
44 J-H. Jean and T. A. Ring, *Proc. Brit. Ceram. Soc.*, *38* (1986) 399.
45 T. E. Mates and T. A. Ring, *Colloids and Surfaces*, *24* (1987) 299.
46 C. Herard, private discussion.
47 J. A. Dirksen, S. Benjelloun and T. A. Ring, *Colloid Polymer Sci.*, *268* (1990) 864.
48 E. Matijevic, in *Advances in Ceramics*, vol. 21, *Ceramic Powder Science and Technology*, The Am. Ceram. Soc., 1987, p. 423.
49 E. Matijevic, in P. Vincenzini (ed.), *High-Tech Ceramics*, Elsevier Science, Amsterdam, 1987, p. 441.
50 T. A. Witten and L. M. Sander, *Phys. Rev. Lett.*, *47* (1981) 1400.
51 R. B. Wilhelmy and E. Matijević, *Colloids Surf.*, *22* (1987) 111.